Correlation between Thermal Properties, Electrical Conductivity, and Crystal Structure in the $BaCe_{0.80}Y_{0.20}O_{2.9}$ Proton Conductor

Lorenzo Malavasi,*[,†,‡] Clemens Ritter,[§] and Gaetano Chiodelli[‡]

Dipartimento di Chimica Fisica, INSTM, CNR−IENI Sezione di Pavia, Università di Pavia, Viale Taramelli 16, I-27100 Pavia, Italy, and Institute Laue-Langevin, Boite Postale 156, F-38042, Grenoble, France

Received November 29, 2007. Revised Manuscript Received January 7, 2008

In this paper, we report an extensive neutron diffraction investigation at high temperature on the $BaCe_{0.80}Y_{0.20}O_{2.9}$ proton conducting material. Our results precisely define the structural evolution of this compound as a function of temperature which evolves from the monoclinic structure found at room temperature to the orthorhombic symmetry (*Imma* space group) at 500 °C; then it adopts a rhombohedral structure from 600 to 700 °C and finally transforms into the more symmetric cubic structure at the highest investigated temperature (800 °C). This progressive increase in the symmetry of the system is not accompanied by any first order phase transition as also confirmed by thermal analysis. Finally, combined neutron data and TGA measurement shows that the oxygen content in the sample is stable up to about 700 °C. Above this temperature, the oxygen content reduces from the nominal content of about 2.9 to about 2.8.

1. Introduction

Many efforts in the field of solid state ionics have focused in the last two decades on the study of perovskite oxides exhibiting significant proton conductivity due to their possible application in solid-state electrochemical devices such as fuel cells, gas sensors, and hydrogen pumps.[1–9] With the progress in the synthesis and characterization of the newly discovered materials, such as the $BaCeO_3$ and $CaZrO_3$ perovskites, an intense research has also been devoted to the comprehension of the defect chemistry of the same materials, in order to optimize their performance and build the basis for the development of other solid-state proton conductors,[10–15] which are recently attractive candidates for applications in intermediate-temperature solid oxide fuel cells (IT-SOFCs). In fact, proton conducting electrolytes for IT-SOFCs have also the advantage of water production at the cathode, thus avoiding the fuel dilution at the anode.

One of these perovskites showing promising properties in the field of solid state proton conductors is the aliovalent-doped barium cerate, $BaCe_{1-x}A_xO_{3-\delta}$ (A = commonly rare earth, $\delta = x/2$). $BaCeO_3$ has been reported to have a total conductivity of about $5.3 \times 10^{-2}\ \Omega^{-1}\ cm^{-1}$ when it is doped with 20% Y ($BaCe_{0.80}Y_{0.20}O_{2.9}$).[14] Guan and co-workers[16] provided evidence for increasing total conductivity in $BaCe_{1-x}Y_xO_{3-\delta}$ with the increase of Y concentration up to $x = 0.2$. The increase in the proton conductivity with doping is mainly related to the creation of oxygen vacancies through the defect reaction (written in Kroger−Vink notation)

$$2Ce_{Ce}^{X} + Y_2O_3 + O_O^X \rightarrow 2Y_{Ce}^{'} + V_O^{\bullet\bullet} + 2CeO_2 \qquad (1)$$

with oxygen vacancies constituting the site for the incorporation of water in the form of hydroxyl groups through

$$H_2O_g + V_O^{\bullet\bullet} + O_O^X \leftrightarrow 2OH_O^{\bullet} \qquad (2)$$

Whereas oxygen vacancies represent the main defects at high temperatures where water molecule desorption and oxygen migration take place in the bulk, the dissolution of protons is favored by decreasing temperatures. In fact, proton incorporation is found to be exothermic, suggesting an energetic stabilization of the protonic defects with increased doping.[17,18]

* Corresponding author. Tel: 39-0382-987921. Fax: 39-0382-987575. E-mail: lorenzo.malavasi@unipv.it.
† Dipartimento di Chimica Fisica, Università di Pavia.
‡ CNR−IENI Sezione di Pavia, Università di Pavia.
§ Institute Laue-Langevin.

(1) Takahashi, T.; Iwahara, H. *Rev. Chim. Miner.* **1980**, *17*, 243.
(2) Iwahara, H.; Uccida, H.; Maeda, N. *Solid State Ionics* **1981**, *359*, 3–4.
(3) Iwahara, H.; Uccida, H.; Ono, K.; Ogaki, J. *J. Electrochem. Soc.* **1988**, *135*, 529.
(4) Norby, T. *Solid State Ionics* **1999**, *125*, 1.
(5) Norby, T.; Widerøe, M.; Glöckner, R.; Larring, Y. *Dalton Trans.,* **2004**, *19*, 3012–3018.
(6) Nowick, A. S.; Du, Y.; Liang, K. C. *Solid State Ionics* **1999**, *125*, 303.
(7) Ito, N.; Iijima, M.; Kimura, K.; Iguchi, S. *J. Power Sources* **2005**, *152*, 200.
(8) Peng, R.; Wu, Y.; Yang, L.; Mao, Z. *Solid State Ionics,* **2006**, *177*, 389–393.
(9) Maffei, N.; Pelletier, L.; Charland, J. P.; McFarlan, A. *J. Power Sources,* **2005**, *140*, 264–267.
(10) Islam, M. S.; Davies, R. A.; Gale, J. D. *Chem. Mater,* **2001**, *13*, 2049–2055.
(11) Wu, J.; Davies, R. A.; Islam, M. S.; Haile, S. M. *Chem. Mater,* **2005**, *17*, 846–851.
(12) Wu, J.; Li, L. P.; Espinosa, W. T. P.; Haile, S. M. *J. Mater. Res.* **2004**, *19* (8), 2366.
(13) Kreuer, K. D. *Annu. Rev. Mater. Res.* **2003**, *33*, 333.
(14) Iwahara, H. *Solid State Ionics* **1995**, *77*, 289.
(15) Higuchi, T.; Tsukamoto, T.; Matsumoto, H.; Shimura, T.; Yashiro, K.; Kawada, T.; Mizusaki, J.; Shin, S.; Hattori, T. *Solid State Ionics* **2005**, *77*, 2967.
(16) Guan, J.; Dorris, S. E.; Balachandran, U.; Liu, M. *J. Electrochem. Soc.* **1998**, *145*, 1780.
(17) Glöckner, R.; Islam, M. S.; Norby, T. *Solid State Ionics* **1999**, *122*, 145.
(18) Kreuer, K. D. *Solid State Ionics* **1999**, *125*, 285.

10.1021/cm7033917 CCC: $40.75
Published on Web 02/20/2008

An extremely relevant aspect of any material that should be used in a device is the investigation of the structural behavior as a function of temperature. In the present literature, it is possible to find exhaustive work related to the high-temperature phase behavior of pure $BaCeO_3$.[19,20] The seminal neutron diffraction work by Knight precisely defined a quite complex trend in the structural evolution of $BaCeO_3$; it was found that this material undergoes three structural phase transitions between 4.2 and 1273 K: (a) from 4.2 to 563 K, it is orthorhombic, with space group *Pnma*; (b) at 563 K, it undergoes a second order phase transition to a second orthorhombic phase with space group *Immm*; (c) at 673 K, it undergoes a first-order phase transition to a rhombohedral structure with space group $R\bar{3}c$; (d) at 1173 K, it transforms to a cubic phase with space group $Pm\bar{3}m$. The same paper discusses as well the structural properties of the $BaCe_{0.90}Y_{0.10}O_{2.95}$ sample, which shows an analogous trend in the crystal structure evolution with temperature as $BaCeO_3$.

The effect of the Y-concentration in $BaCe_{1-x}Y_xO_{3-\delta}$ solid solution for $0 \leq x \leq 0.3$ is considered in response to heat treatments in oxidizing, reducing, and water-vapor containing atmospheres in ref 21. However, the neutron diffraction data reported refer only to room-temperature patterns.

To the best of our knowledge the only paper reporting some high-temperature neutron data compassing also the $BaCe_{0.80}Y_{0.20}O_{2.9}$ material is a recent work by C.-K. Loong et al.[22] This paper provides some information about the temperature evolution of the $BaCe_{1-x}Y_xO_{3-\delta}$ solid solution for $0 \leq x \leq 0.3$ but it is mainly devoted to the description of the application of small-to-wide angle diffraction and inelastic scattering for the investigation of this system without providing a detailed study of the high temperature structural evolution and features of $BaCe_{0.80}Y_{0.20}O_{2.9}$. In view of these considerations, we believe that a detailed and deep investigation analysis of the $BaCe_{0.80}Y_{0.20}O_{2.9}$ proton conductor is highly demanded. For this purpose we carried out a neutron diffraction investigation of BCY as a function of temperature between room temperature (RT) and 800 °C. In addition, in order to further support the results of the neutron diffraction investigation we completed the structural study with thermal analysis and electrical conductivity measurements. In particular, thermogravimetry (TGA) was used to probe the oxygen content stability of $BaCe_{0.80}Y_{0.20}O_{2.9}$ in the investigated temperature range while the differential scanning calorimetry (DSC) was used to asses the nature of the observed structural phase transition. Finally, the transport properties of $BaCe_{0.80}Y_{0.20}O_{2.9}$ in the same environment and *T*-range of the other measurements was followed to possible correlate the σ versus T trend with variation in the crystal structure of the material.

2. Experimental Section

Powder samples of $BaCe_{0.80}Y_{0.20}O_{2.9}$ have been prepared by conventional solid state reaction from the proper stoichiometric amounts of BaO, CeO_2, and Y_2O_3 (all Aldrich, ≥99.9%) by two successive firings for 20 h at 1200 °C. X-ray diffraction analysis collected on a Bruker D8 Advance diffractometer (Cu radiation, 2θ-range 10–110°, step size 0.02°, time per step 5 s) was used for assessment of phase purity of the as synthesized material. No traces of spurious phases have been detected.

The chemical composition was checked by means of microprobe analysis which revealed a sample composition in agreement with the nominal one.

Neutron powder diffraction (NPD) patterns were acquired on the D1A instrument at the Institute Laue Langevin (ILL) in Grenoble. All measurements were recorded in static air in a silica glass container. The diffraction patterns were collected in the angular range 0−160°, step 0.05°, at a wavelength 1.39 Å, for about 6 h per spectrum in the temperature range between room temperature and 800 °C every 100 °C.

All the neutron diffraction patterns were analyzed according to the Rietveld method[23,24] by means of the FULLPROF software package.[25] Cell parameters, atomic position, and isotropic thermal factors for the cations and anisotropic thermal factors for the oxygen ions were refined. The background coming from the empty quartz tube was recorded at the same temperatures and subtracted from the NPD patterns of the samples.

AC electrical characterizations were made by using the Impedance Spectroscopy (IS) technique with a frequency response analyzer (FRA) Amel 7200 or Solatron 1260 apparatus, in the frequency range 10^{-3}–10^7 Hz. A homemade high-impedance adapter (up to 1×10^{13} ohm, 2 pF) with an active guard driver was applied to the FRA in order to reduce the noise and the parasitic capacitances of cables and cells and to increase the sensitivity and input impedance of the apparatus. High-temperature measurements (up to 900 °C) were performed by inserting the electrochemical cell in an oven under static air. To ensure good electrical contact for AC measurements, we deposited platinum layers by sputtering on the flat surfaces of the pellets. The pellets (10 mm in diameter) for the electrical conductivity measurements were prepared by axially pressing the resulting powders and sintering them at 1300 °C for 10 h. The density of the final pellet was greater than 95%.

Thermogravimetry (TGA) measurements were carried out under the same conditions as the diffraction measurements (i.e., in static air) from RT to 800 °C with a heating rate of 5 °C/min with a TA2950 instrument. Differential scanning calorimetry (DSC) were carried out in static air as well on the powdered samples using a SDT2960 TA instrument in the range 25–800 °C at a heating rate of 5 °C/min.

3. Results and Discussion

3.1. Crystal Structure Evolution of BCY with *T*. Figure 1 displays the neutron diffraction (ND) patterns acquired on the $BaCe_{0.80}Y_{0.20}O_{2.9}$ sample at the different temperatures investigated (30–800 °C). The inset highlights a region showing clear changes. As already previously stated, neutron diffraction is a more sensitive probe with respect to X-ray diffraction for the study of cerates due to both the possibility to get valuable information related to superlattice intensity and for the lack of form-factor fall with Q.[20]

(19) Knight, K. S. *Solid State Ionics* **1994**, *74*, 109.
(20) Knight, K. S. *Solid State Ionics* **2001**, *145*, 275.
(21) Takeuchi, K.; Loong, C.-K.; Richardson Jr, J. W.; Guan, J.; Dorris, S. E.; Balachandran, U. *Solid State Ionics* **2000**, *138*, 63.
(22) Loong, C.-K.; Ozawa, M.; Takeuchi, K.; Ui, K.; Koura, N. *J. Alloys Compd.* **2006**, *1065*, 408–412.
(23) Rietveld, H. M. *Acta Crystallogr.* **1967**, *22*, 151.
(24) Rietveld, H. M. *J. Appl. Crystallogr.* **1969**, *2*, 65.
(25) Rodriguez-Carvajal, J. *Physica B* **1993**, *192*, 55.

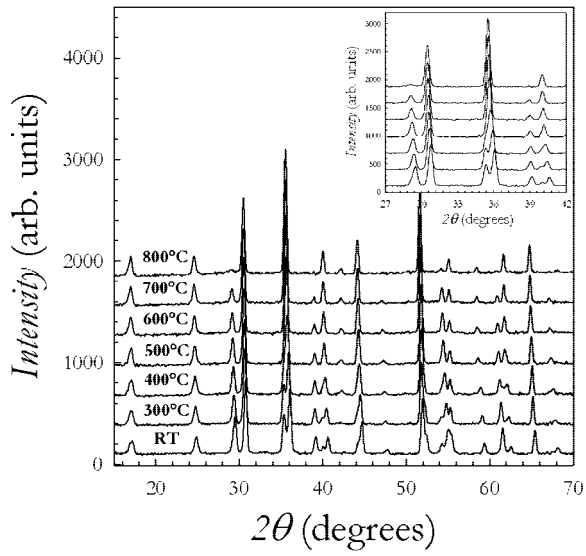

Figure 1. Neutron diffraction (ND) patterns of BCY at the temperatures investigated. Inset: details of ND patterns around the region where main peaks are located. Temperatures are the same as in the main figure.

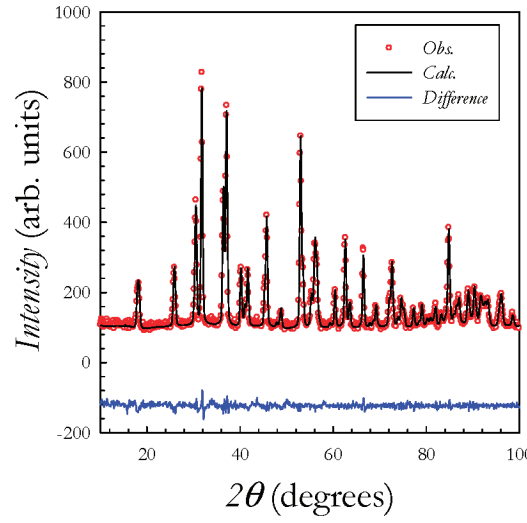

Figure 2. Rietveld refined neutron diffraction pattern for BCY at room temperature: observed, calculated, and difference profile.

The simple visual inspection of the pattern changes with temperature suggests an increase of symmetry by increasing temperature and, in addition, that the structural changes occur gradually with temperature. Just to make some representative examples, the main peak, located at about 36°, is found to be split at RT and progressively becomes a single peak at 600 °C; in the same way the three peaks between 38 and 42° first merge in 2 peaks at 500 °C and then just one peak is left at 800 °C.

For all the temperatures the validity of the proposed crystal structures was first checked by means of a matching-profile fit followed by Rietveld refinement. For the data at RT, it was found that the correct description of the observed pattern is consistent with a monoclinic unit cell belonging to the *I*2/*m* space group (No. 12). In addition, about 7% of a secondary phase has been detected. The nature of this secondary phase can not easily assessed because for both the rhombohedral and orthorhombic phases (*Imma* or *Pnma*) the main peaks are located more or less at the same position. The best χ^2 (5.4) was obtained by including in the refinement a secondary phase with the orthorhombic *Imma* symmetry (lattice parameter: $a = 6.2367(2)$, $b = 8.7679(3)$ and $c = 6.2435(2)$), whereas for other crystal structures, the χ^2 was always greater than 6. The final refinement of the RT ND pattern is shown in Figure 2. Structural data for the monoclinic phase are reported in Table 1.

The monoclinic structure has been found also at 300 and 400 °C. In Figure 3, it is reported the trend of the pseudocubic cell volume while in Figure 4 it is reported the behavior of the lattice parameters as a function of temperature. As can be appreciated the cell volume expands linearly with temperature. The lattice constants reported in Figure 4 have been expressed in terms of a pseudocubic cell, neglecting the small monoclinic distortion (β angle $\neq 90$). The three lattice parameters tend to get closer as the temperature increases and this is particularly evident for the a and c lattice constants. The evolution of the monoclinic β angle with temperature is reported in Figure 5. As the temperature increases, the distortion of the unit cell is reduced as witnessed by the β angle moving progressively closer to 90°.

At 500 °C, the BCY neutron pattern can not be modeled anymore with a monoclinic structure. In particular, in the region of the main peak (around 36°) the previously observed splitting of the (−202) and (202) reflections, due to the deviation of the β angle from 90°, has disappeared and a single symmetric peak is now present. Several other examples of splitting removal are present in the pattern.

According to the only available high-temperature structural study realized on $BaCe_{0.80}Y_{0.20}O_{2.9}$,[22] at 500 °C the structure should be, mainly, in the *Pnma* orthorhombic phase (under oxidative atmosphere). However, this crystal structure is not compatible with our diffraction pattern. Figure 6 reports a simulation of the expected diffraction pattern in the case of a *Pnma* and in the case of a *Imma* orthorhombic structure. As can be appreciated, the experimental pattern at 500 °C does not display those peculiar reflections of the *Pnma* symmetry which are partially (only the most intense ones) highlighted in the bottom part of Figure 6 with arrows. The pattern at 500 °C has been also checked with respect to the rhombohedral $R\bar{3}c$ symmetry. The presence of some peak splitting in the experimental NPD pattern at high angles (particularly above 75°) together with some peak broadening clearly rule out the presence of the rhombohedral symmetry at this temperature. The collected evidence totally support the formation of an *Imma* orthorhombic phase at 500 °C. We finally note that the *Imma* space group and the *I*2/*m* monoclinic space group are correlated by a group-subgroup relation. The quality of the refinement of neutron data at this temperature with the proposed structure can be inferred by looking at Figure 7.

The pseudocubic cell volume, the lattice parameters. and the refinement results are reported, respectively, in Figures 3 and 4 and Table 1. From Figure 3, we note that there are no detectable discontinuities in the cell volume trend at the *I*2/*m* → *Imma* phase transition. This suggest a second-order phase transition, which is in agreement with a group−subgroup

Table 1. Structural Data for $BaCe_{0.80}Y_{0.20}O_{2.9}$ at the Different Temperatures Investigated

		RT	300 °C	400 °C	500 °C	600 °C	700 °C	800 °C
space group		*I2/m*	*I2/m*	*I2/m*	*Imma*	$R\bar{3}c$	$R\bar{3}c$	$Pm\bar{3}m$
a (Å)		6.2487(1)	6.2579(1)	6.2589(1)	6.2568(6)	6.26424(6)	6.27138(6)	4.4359(2)
b (Å)		8.7419(1)	8.7817(1)	8.8037(2)	8.8268(7)	6.26424(6)	6.27138(6)	4.4359(2)
c (Å)		6.2339(1)	6.2538(1)	6.2588(1)	6.2711(6)	15.34041(2)	15.35102(2)	4.4359(2)
β (deg)		90.9962(9)	90.8489(9)	90.498(1)				
V (Å^3)		340.50(8)	343.64(8)	344.8(1)	346.34(6)	521.3(1)	522.8(1)	87.288(9)
Ba	*x*	0.262(1)	0.256(2)	0.252(3)	0	0	0	0.5
	y	0	0	0	0.25	0	0	0.5
	z	0.737(1)	0.736(2)	0.736(3)	0.995(2)	0.25	0.25	0.5
	B	1.5(1)	2.1(1)	1.9(1)	2.4(1)	2.7(1)	3.0(1)	4.0(2)
Ce/Y	*x*	0.25	0.25	0.25	0	0	0	0
	y	0.25	0.25	0.25	0	0	0	0
	z	0.25	0.25	0.25	0.5	0	0	0
	B	0.47(9)	0.7(1)	1.0 (1)	0.77(8)	1.11(8)	1.30(9)	1.7(1)
O1	*x*	0.183(1)	0.193(2)	0.194(2)	0	0.4515(4)	0.4573(6)	0
	y	0	0	0	0.25	0	0	0.5
	z	0.228(1)	0.225(2)	0.239(3)	0.435(1)	0.25	0.25	0
	B	2.35(9)	4.3(1)	4.5(1)	3.0(1)	3.6(2)	4.2(2)	6.5(3)
O2	*x*	0	0	0	0.25			
	y	0.310(1)	0.302(2)	0.298(2)	0.5317(7)			
	z	0	0	0	0.25			
	B	2.5(1)	2.9(1)	2.8(2)	3.4(1)			
O3	*x*	0.5	0.5	0.5				
	y	0.2241(9)	0.226(1)	0.225(2)				
	z	0	0	0				
	B	2.0(1)	3.0(1)	3.6(2)				

relationship between the two phases and with the continuous and progressive reduction of structure distortion from RT to 500 °C. In addition, no clear calorimetric peaks are found in correspondence of this transition (see later in the text).

The further raise of temperature to 600 °C leads to the appearance of a new crystal structure. This is well-witnessed by the reduction of peak broadening and removal of several peak splittings which is particularly evident at high angle (see inset of Figure 7b). The new crystal structure adopted by the $BaCe_{0.80}Y_{0.20}O_{2.9}$ sample is the $R\bar{3}c$ rhombohedral structure. The refinement of the ND experimental pattern at this temperature is shown in the main part of Figure 7b. The pseudocubic cell volume, the lattice parameters and the refinement results at 600 °C are reported, respectively, in Figures 3 and 4 and Table 1. No sign of any secondary phase is found. The *Imma* → $R\bar{3}c$ phase transition does not occur with any evident discontinuity in the pseudocubic cell volume. This is in contradiction with a previous report by Knight on the $BaCeO_3$ material,[19] in which it was shown a significant discontinuity in the cell volume trend of about 0.5% at this phase transition. However, our results are in agreement with those reported in a neutron diffraction study on the $BaCe_xZr_{1-x}O_3$ solid solution[26] and in agreement with a previous work on the Raman spectroscopy properties of pure $BaCeO_3$.[27] We may note, however, that to the best of our knowledge, this is the first paper reporting the structural details, as a function of temperature, for the $BaCe_{0.80}Y_{0.20}O_{2.9}$ sample and that significant differences may be present with respect to the pure compound. For the 10% Y-doping, Knight found the same sequence of phase transitions of the pure samples but with modified widths of the phase field.[20] The

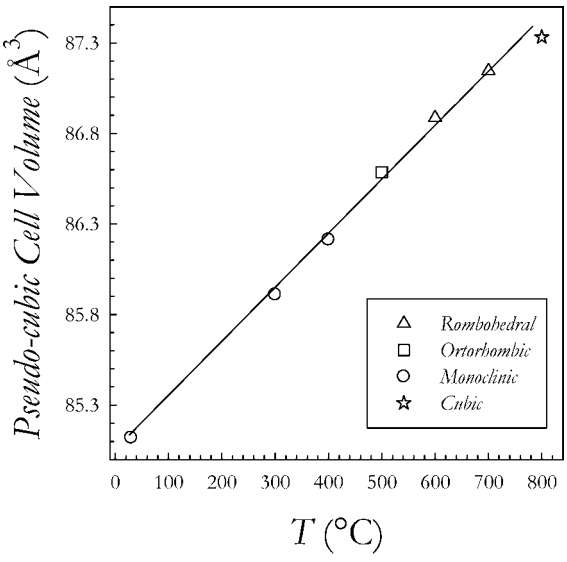

Figure 3. Pseudocubic cell volume as a function of temperature for BCY. Error bars are smaller than symbols.

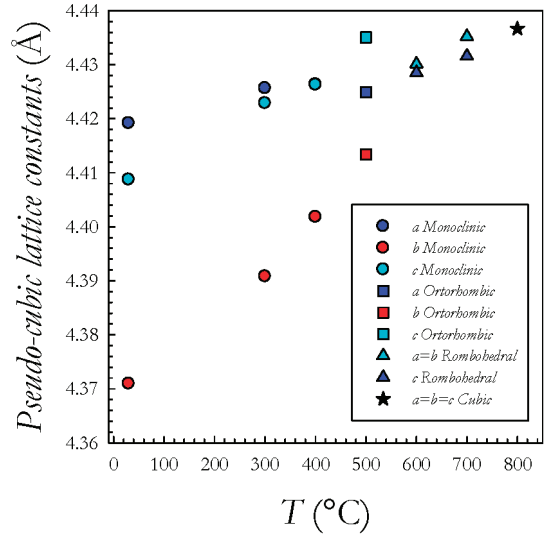

Figure 4. Lattice constants as a function of temperature for BCY. Error bars are smaller than symbols. For rhombohedral and orthorhombic, samples are reported the pseudocubic lattice parameters.

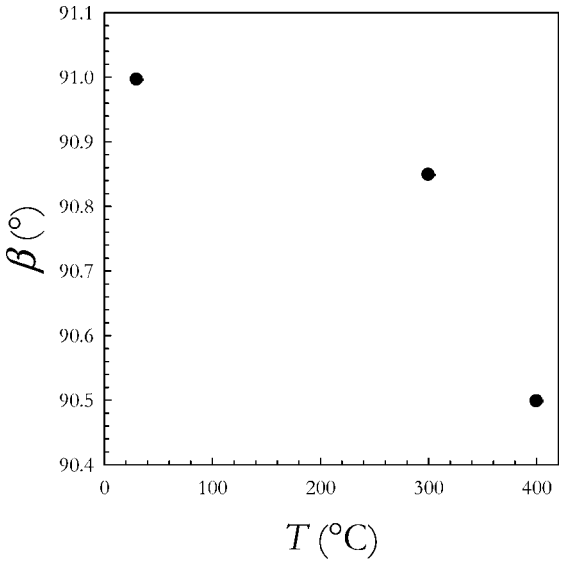

Figure 5. Monoclinic β angle variation as a function of temperature for BCY. Error bars are smaller than symbols.

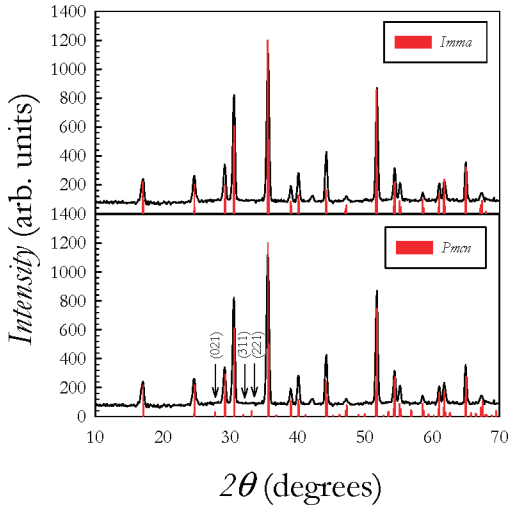

Figure 6. Comparison between experimental pattern a 500 °C (black line) and calculated diffraction patterns for the *Pmcn* (bottom panel) and *Imma* (top panel) orthorhombic structures.

further increase of Y-doping leads to a different sequence of structural changes without the observed discontinuity in the cell-volume trend found previously for pure $BaCeO_3$.

The rhombohedral structure is also found at 700 °C. Again, the pseudocubic cell volume, the lattice parameters and the refinement results at this temperature are reported, respectively, in Figures 3 and 4 and Table 1.

As can be appreciated from Figure 1, at 800 °C, the BCY structure undergoes a further symmetrization as clearly evidenced by the reduction of Bragg peaks found in the pattern. The crystal structure adopted at this temperature is the $Pm\bar{3}m$ cubic structure. This result agrees with the results found by Knight, where for the pure $BaCeO_3$, the cubic structure is observed at 900 °C.[20] The refined pattern is shown in Figure 7c. Beside the cubic phase a second rhombohedral phase has been added in the refinement. The amount of the latter, according to the refinement results, was 1.2(2)%. Structural parameters are reported in Figure 3, 4 and Table 1. As for the previous cases, we did not observe any strong discontinuity in the unit-cell volume at the $R\bar{3}c \rightarrow Pm\bar{3}m$ phase transition, although a deviation from the linear behavior with T observed for the data up to this temperature can be inferred at 800 °C from Figure 3. The origin of this slight deviation is not easily assessed since the $BaCe_{0.80}Y_{0.20}O_{2.9}$ compound undergoes oxygen content loss with increasing temperature (particularly above 700 °C, see later in the text) as well as a progressive change in the Ce oxidation state which may lead to a nonlinear trend in the V versus T data. From the structural and calorimetric data it is possible to conclude that this phase transition is of second order. Finally, it is worth to comment that the structural changes observed in the present paper relates to the average structure of the material, as probed by means of neutron diffraction. It would be interesting to follow the evolution of the local structure as well by means of a technique such as the total neutron scattering, which we have already previously applied to an oxygen conducting materials[28] and has several advantages over the X-ray absorption spectroscopy.[29]

3.2. Evolution of the Structural Parameters with *T*. From the Rietveld refinements, we calculated the bond lengths and bond angles at the different temperatures explored. Figure 8 displays the average Ba−O and Z−O bond lengths (Z = Ce and Y) as a function of temperature for $BaCe_{0.80}Y_{0.20}O_{2.9}$. Regarding the Z−O bond, there are three distinct lengths in the monoclinic structure, two in the orthorhombic and one in the rhombohedral and cubic crystal structures. It can be appreciated that the temperature evolution of the Z−O and Ba−O bond lengths is opposite: in the first case, there is a progressive contraction of the bond length as the temperature increases with a severe contraction at 800 °C, whereas in the second case, the bond length expands up to 700 °C and then slightly shrinks from 700 to 800 °C. An analogous result was found previously in ref 26 for the $BaCe_xZr_{1-x}O_3$ solid solution and was interpreted in term of a reduction of tilt by increasing temperature.

On the basis of the average bond lengths derived from the Rietveld refinements, we calculated the geometrical tolerance factor (t)

$$t = \frac{\langle \mathrm{Ba-O} \rangle}{\sqrt{2}\langle \mathrm{Z-O} \rangle} \qquad (3)$$

which is a measure of the distortion degree of a perovskite compound. The results are summarized in the inset of Figure 8. The value of t progressively increases from RT to 800 °C as the perovskite structure becomes more and more regular. The values of the bond lengths are reported in Table 2.

The temperature evolution of the average Z−O−Z bond angle and the <Ba−Z> bond length are reported in Figure 9. In agreement with the increase in the symmetry of the perovskite structure, the bond angle moves from about 155°

(26) Pagneir, T.; Charrier-Cougoulic, I.; Lucazeau, G. *Eur. Phys. J. AP* **2000**, *9*, 1.
(27) Genet, F.; Loridant, S.; Lucazeau, G. *J. Raman Spectrosc.* **1997**, *28*, 255.
(28) Malavasi, L.; Kim, H.; Billinge, S. J. L.; Proffen, Th.; Tealdi, C.; Flor, G. *J. Am. Chem. Soc.* **2007**, *129*, 6903.

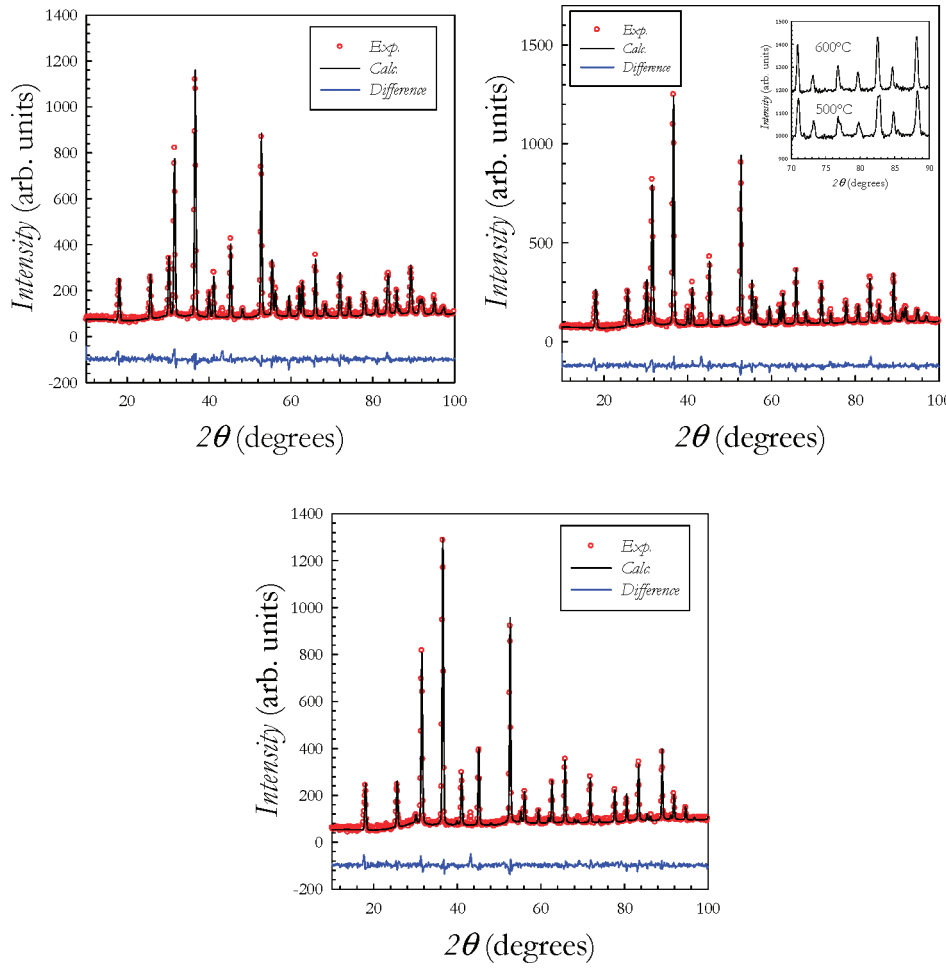

Figure 7. (a) Rietveld refined neutron diffraction pattern for BCY at 500 °C: observed, calculated and difference profile. (b) Rietveld refined neutron diffraction pattern for BCY at 600 °C: observed, calculated, and difference profile. Inset: comparison of a selected region of the ND patterns at 500 and 600 °C. (c) Rietveld refined neutron diffraction pattern for BCY at 800 °C: observed, calculated, and difference profile.

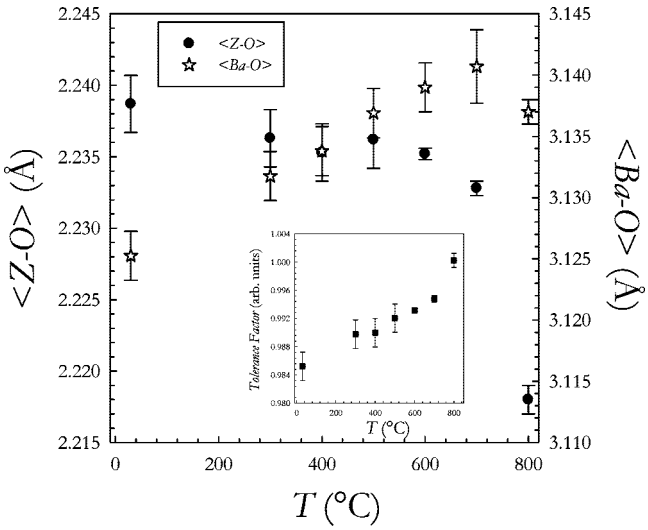

Figure 8. Average Z−O (full circles) and Ba−O (empty stars) bond lengths evolution with temperature for BCY. Inset: tolerance factor variation with *T*.

to 180°. Let us remember that in the monoclinic and orthorhombic structures, there are two distinct Z−O−Z bond angles (one within the equatorial plane and the other in the axial plane). The values of the two angles are reported in Table 2 together with the Ba−Z average bond length. In addition, as the Z−O environment becomes more compact by reduction of the bond length the distance between the cations increases linearly with temperature by about 0.8%.

Figure 10 shows the temperature variation of the atomic displacement parameters (a.d.p.) for the BCY compound. For the oxygen ions we modeled the adp by means of an anisotropic thermal factor. In the Figure it is reported the resulting isotropic parameter (*B*). The overall behavior shows a progressive increase in all the *B* parameters as the temperature increases without any significant anomaly except for a quite significant rise of the O adp at 800 °C. This can be correlated to the high mobility of oxygen ions at high temperature in the $BaCe_{0.80}Y_{0.20}O_{2.9}$ material.

Finally, Figure 11 reports the variation of the oxygen content as derived from the refinement of the oxygen atoms occupancies. In the figure, we also plotted a thermogravimetric trace of $BaCe_{0.80}Y_{0.20}O_{2.9}$ collected under the same experimental conditions employed for the acquisition of the neutron diffraction patterns. First of all, we note that the refined occupancy at RT is around 2.90(4), in good agreement with the nominal oxygen content of the sample. This oxygen content remains practically constant until about 600

(29) Egami, T. Billinge, S. J. L. *Underneath the Bragg Peaks: Structural Analysis of Complex Materials*; Pergamon Press: Oxford, U.K., 2003.

Table 2. Bond Lengths and Angles for $BaCe_{0.80}Y_{0.20}O_{2.9}$ at the Different Temperatures Investigated

	RT	300 °C	400 °C	500 °C	600 °C	700 °C	800 °C
params	*I*2/*m*	*I*2/*m*	*I*2/*m*	*Imma*	$R\bar{3}c$	$R\bar{3}c$	$Pm\bar{3}m$
Z−O1 (Å)	2.228(2)	2.229(2)	2.230(2)	2.244(2)	2.235(4)	2.233(5)	2.218(1)
Z−O2 (Å)	2.251(3)	2.242(3)	2.243(3)	2.232(5)			
Z−O3 (Å)	2.237(1)	2.238(1)	2.233(2)				
Z−O1−Z (deg)	157.49(7)	159.99(9)	161.59(7)	159.13(6)	164.40(1)	166.25(1)	180
Z−O2−Z (deg)	152.82(8)	156.50(8)	158.30(8)	165.60(3)			
<Ba-O> (Å)	3.125(2)	3.122(2)	3.1334(2)	3.137(2)	3.139(2)	3.141(3)	3.137(1)
<Ba-Z> (Å)	3.811(1)	3.822(1)	3.826(1)	3.829(2)	3.836(1)	3.838(1)	3.842(1)
t	0.985	0.989	0.990	0.992	0.993	0.995	1
R_{wp}	6.35	7.1	7.9	7.2	7.2	7.8	7.1
χ^2	4.05	4.9	5.1	4.5	3.6	4.6	3.9

°C and then starts to decrease. The oxygen content derived from oxygen occupancy at 800 °C is 2.79(4). The comparison with the TGA trace reveals a good overlap between the weight variation and the oxygen content change with temperature. The weight change in the thermogravimetric measure is ascribable to the change in the oxygen content only. This can be concluded by the reversible behavior of the weight variation with *T* (not shown). The oxygen content at 800 °C determined from the TGA curve is 2.82, which is in fairly good agreement with the oxygen content determined from the Rietveld refinement.

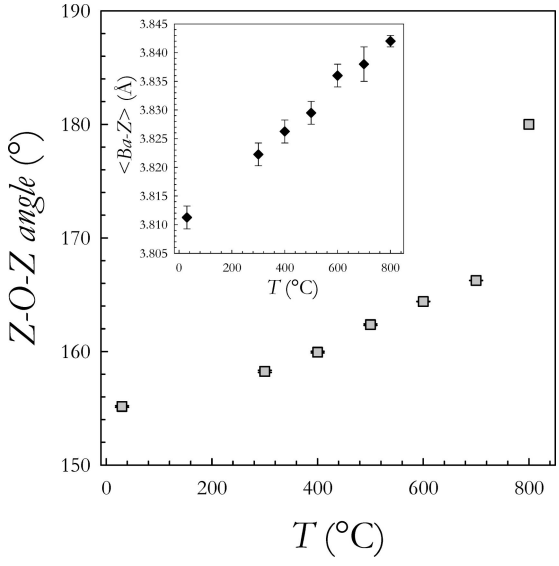

Figure 9. Evolution of the average Z−O−Z bond angle with temperature for BCY. Inset: <Ba−Z> bond length variation as a function of temperature.

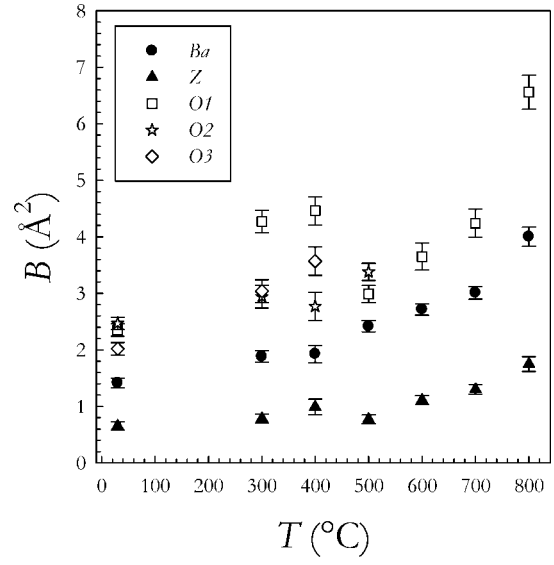

Figure 10. Evolution of the atomic displacement parameters for BCY compound as a function of temperature.

Regarding the localization of the oxygen vacancies, we could observe that the O1 site in the monoclinic structure, i.e., the apical oxygen, always resulted in being fully occupied within the experimental error, whereas the O2 and O3 sites, i.e., the equatorial oxygens, showed partial occupancies, particularly in the O2 site. A sketch of the monoclinic structure with the atom labels is reported in Figure 12a. Even though there are no previous studies on monoclinic phases of doped barium cerates, the result of oxygen vacancies mainly located on the equatorial plane is in good agreement with a similar work by Kruth et al. on the orthorhombic $Ba_{1-x}La_xCe_{0.9-x}Y_{0.1+x}O_{2.95}$ solid solution[30] where, by means of combined experimental and computational techniques, it was found that the preferential site for the oxygen vacancy location mainly involves the O2 site (i.e., the equatorial oxygen of the orthorhombic crystal structure). In ref 30 it was also found that for the BCY material with a high density of oxygen vacancy the water incorporation energy (E_{H_2O}) is more exothermic for water incorporation at the O2 position. Also in the present case, for the orthorhombic phase of $BaCe_{0.80}Y_{0.20}O_{2.9}$, the oxygen occupancy was found to be complete for the O1 site and partial

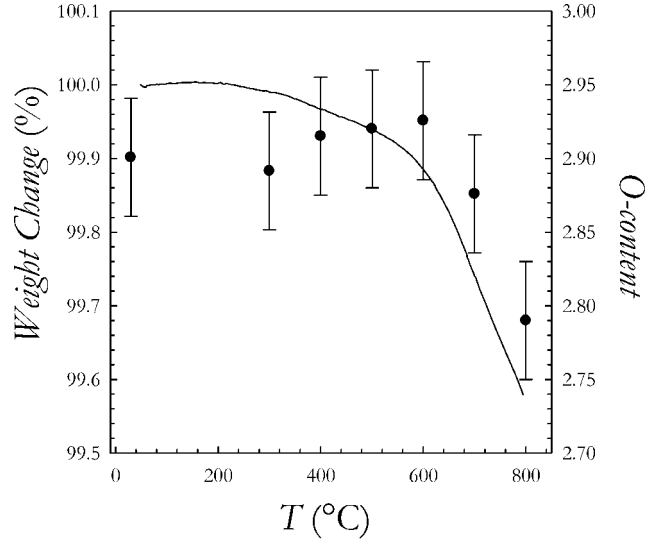

Figure 11. TGA trace of $BaCe_{0.80}Y_{0.20}O_{2.9}$ sample under air (solid line) and oxygen content as a function of temperature as determined from the refinement of the oxygen occupancy.

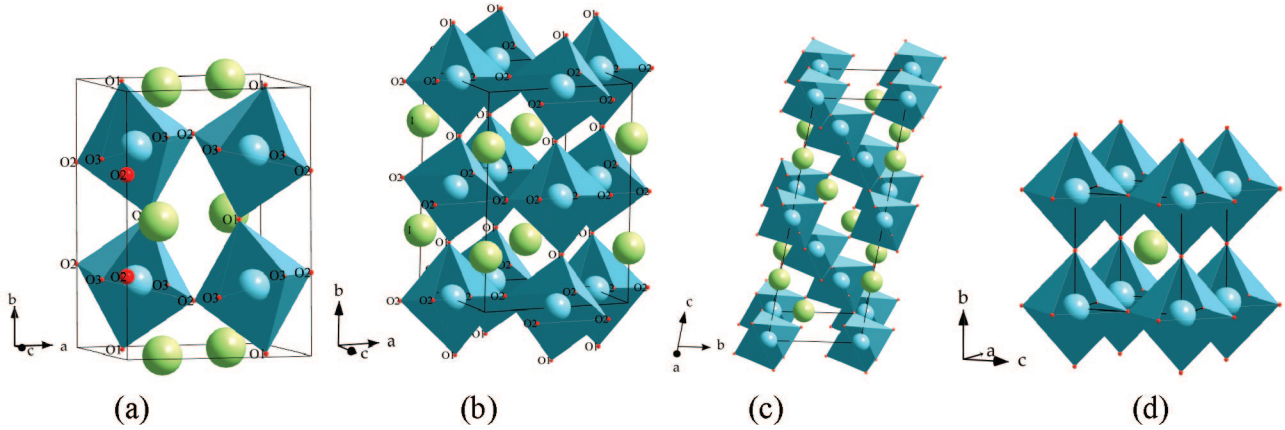

Figure 12. Sketch of the $BaCe_{0.80}Y_{0.20}O_{2.9}$ crystal structure as a function of temperature with Z−O polyhedra. Green spheres, Ba ions; blue spheres, Y/Ce ions; red spheres, oxygen ions. Where more than one O site was present in the structure, the oxygen sites were labelled according to the corresponding crystal structure.

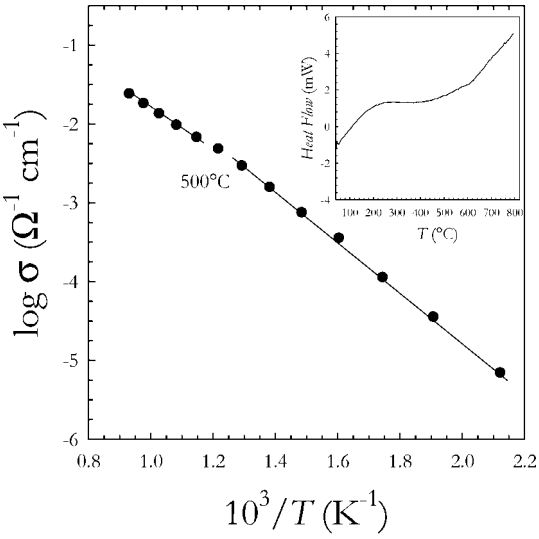

Figure 13. Arrhenius plot of electrical conductivity in air for $BaCe_{0.80}Y_{0.20}O_{2.9}$. Inset: DSC trace of $BaCe_{0.80}Y_{0.20}O_{2.9}$.

for the O2 site. Figure 12b reports a sketch of the *Imma* structure found at 500 °C for the $BaCe_{0.80}Y_{0.20}O_{2.9}$ sample. For sake of completeness, we also plotted in panels c and d of Figure 12 the rhombohedral and cubic structures, respectively.

3.3. Correlation with Transport Properties. Figure 13 displays the Arrhenius plot of the electrical conductivity data of the $BaCe_{0.80}Y_{0.20}O_{2.9}$ sample collected under the same conditions as the neutron diffraction experiments. The conductivity increases as the temperature increases with an evident slope change around 500 °C. The activation energies before and after the slope change are about 0.85 and 0.35 eV, respectively. The data presented in the plot refer to the total conductivity of the sample, which includes both ionic and electronic conductivity. It is known that $BaCe_{0.80}Y_{0.20}O_{2.9}$ has also a small contribution from electronic defects that may play a significant role at high temperature. The identification of the mobile species as a function of temperature is beyond the scope of the present paper. However, the relevant information we can present from our investigation is that the observed change in the activation energy falls in the region of a phase transition of $BaCe_{0.80}Y_{0.20}O_{2.9}$ (*Imma* → $R\bar{3}c$). The trend in the conductivity data coupled to the structural evidence suggests that this transition is of second order in nature. This is also supported by the calorimetric measurements we carried out on the sample under the same conditions of NPD and electrical transport measurements. The DSC trace of $BaCe_{0.80}Y_{0.20}O_{2.9}$ is reported in the inset of Figure 13. As can be appreciated there are no clear peaks witnessing an exo or endothermic thermal event associated with any structural phase transition. This allows us to suggest that the slope change observed in the electrical conductivity data might be associated with an increase in the perovskite structure symmetry which is coupled to the *Imma* → $R\bar{3}c$ transition. However, we may not discard that the slope change could be also associated with a change in the carrier nature as a function of temperature. Further work is planned in order to reveal the exact nature of this behavior.

Conclusions

In this work, we aimed at presenting the structural evolution with temperature of the $BaCe_{0.80}Y_{0.20}O_{2.9}$ proton conducting oxide. To the best of our knowledge, this is the first high-temperature investigation on this stoichiometry, which represents the one displaying the optimal conductivity performance.[2,16] Previous completed NPD works concentrated on pure $BaCeO_3$,[20,31] whereas the only available paper on $BaCe_{0.80}Y_{0.20}O_{2.9}$ did not report any detailed structural insight into the temperature evolution of the material.[21]

The structural results allowed us to define the evolution of the crystal structure of $BaCe_{0.80}Y_{0.20}O_{2.9}$ as a function of temperature. It can be summarized in the following:

(a) from RT to 400, it is monoclinic with space group *I*2/*m*;

(b) at 500 °C, the materials adopts the orthorhombic *Imma* structure;

(c) at 600 and 700 °C, it is rhombohedral ($R\bar{3}c$); and

(d) finally, at 800 °C, it becomes cubic ($Pm\bar{3}m$).

(30) Kruth, A.; Davies, R. A.; Islam, M. S.; Irvine, J. T. S. *Chem. Mater.* **2007**, *19*, 1239–1248.
(31) Genet, F.; Loridant, S.; Ritter, C.; Lucazeau, G. *J. Phys. Chem. Solids* **1999**, *60*, 2009–20021.
(32) Glazer, A. M. *Acta Crystallogr., Sect. B* **1972**, *28*, 3384.
(33) Woodward, P. M. *Acta Crystallogr., Sect. B* **1997**, *53*, 32–43.

As the temperature increases, the octahedral tilting progressively reduces. In the monoclinic structure we are facing a two-tilt system known, in the Glazer's notation[32] as $a^{\circ}b^{-}c^{-}$. The $I2/m \rightarrow Imma$ phase transition makes the tilt around the *z*-axis the same as around the *y*-axes, because it can be written as a $a^{\circ}b^{-}c^{-} \rightarrow a^{\circ}b^{-}b^{-}$ transition. Again, we are in a two-tilt system. Further increase of temperature to 600 °C removes one tilting bringing the symmetry of the system to the $a^{-}a^{-}a^{-}$ tilt system, i.e., the rotation angle is the same about each of the three axes with rotations of two neighboring octahedra, along the tilt axis, which are in opposite directions. Finally, the transition to the cubic $Pm\bar{3}m$ space group is described as a $a^{\circ}a^{\circ}a^{\circ}$ tilt system, which excludes any tilting between octahedra.

This progressive increase in the symmetry of the system is not accompanied by any first-order phase transition. This can be concluded from the thermal analysis carried out on the sample under the same conditions as the NPD acquisition (see Figure 13) and is supported by the absence of any relevant discontinuity in the cell-volume evolution with temperature. A slight deviation of the cell volume at high temperature is most probably related to the variation of the oxygen content above 700 °C (see Figure 11).

Combined neutron data and TGA measurement shows that the oxygen content in the sample is stable up to about 700 °C. Above this temperature the oxygen content reduces from the nominal content of about 2.9 to about 2.8. The oxygen vacancies are preferentially located in the equatorial positions of the BO_6 octahedron. In addition, for the monoclinic structure, the O2 site seems to be the preferential site for the localization of oxygen vacancies. Our results provide direct evidence that the $BaCe_{0.80}Y_{0.20}O_{2.9}$ proton conducting oxide is a stable material without any volume discontinuity within the operational range of an intermediate fuel cell which is a fundamental prerequisite for the incorporation of an electrolyte within a device.

Acknowledgment. This work has been supported by the "Celle a combustibile ad elettroliti polimerici e ceramici: dimostrazione di sistemi e sviluppo di nuovi materiali" FISR Project of Italian MIUR. We recognize the support of the UNIPV-Regione Lombardia Project on Material Science and Biomedicine. The ILL neutron facility and European Community financial support is acknowledged.

CM7033917